# Far-Infrared Absorption of ZnS:$Fe^{2+}$ in Strong Magnetic Fields

J. T. VALLIN AND G. A. SLACK
*General Electric Research and Development Center, Schenectady, New York 12301*
AND
C. C. BRADLEY*
*Francis Bitter National Magnet Laboratory, Massachusetts Institute of Technology, Cambridge, Massachusetts 02139*
(Received 15 July 1970)

We have investigated several optical transitions between the $^5E$ energy levels of the orbital ground state of substitutional $Fe^{2+}$ in natural crystals of cubic ZnS for magnetic inductions up to 14 T (140 kG) at liquid-He temperatures. In these experiments we have used both gas lasers and a Fourier-transform Michelson spectrometer covering the range 10–100 $cm^{-1}$ wave numbers. The results show that simple crystal-field theory is adequate to account for the observed energy levels and their oscillator strengths as a function of the applied magnetic field. There is also evidence for local modes at 43 and 63 $cm^{-1}$ wave numbers caused by trace impurities other than Fe.

## I. INTRODUCTION

Far-infrared absorption has been used to study low-energy electronic levels of $Fe^{2+}(3d^6)$ point defects in crystals of cubic ZnS [1] and CdTe.[2] For ZnS the results could be understood by using simple crystal-field theory. For CdTe, however, additional lines were observed. The presence of these extra lines has been accounted for by including a Jahn-Teller coupling between the electronic states of $Fe^{2+}$ and low-frequency vibrational modes of the CdTe lattice.[3]

The purpose of this investigation is to test crystal-field-theory predictions for ZnS:$Fe^{2+}$ in greater detail and attempt to determine if Jahn-Teller effects can be neglected or not. It is our conclusion that Jahn-Teller effects are not needed to describe the $^5E$ energy levels and the magnetic-field dependence of the oscillator strengths of optical transitions between these levels for $Fe^{2+}$ in ZnS. These results are consistent with predictions of conventional crystal-field theory. However, the Jahn-Teller coupling may have a noticeable effect on the absolute values of the oscillator strengths in that transition probabilities will be shared between no-phonon and one-phonon states.

In this paper we first describe the experimental techniques in Sec. II, and present the experimental results in Sec. III. In Sec. IV we briefly review the predictions of crystal-field theory including the Zeeman splitting. In the same section we also discuss how the oscillator strengths change with magnetic field. In the final section, Sec. V, a comparison between experiment and theory is made.

## II. EXPERIMENTAL

The samples used in the present study were natural single crystals of cubic ZnS, see Table I. The magnetic-field experiments were made on samples *SA* and *SB* from Santander, Spain. These samples have a relatively low Cd concentration as compared to natural crystals from other parts of the world. As we will discuss later, the Cd gives rise to a local mode at 63 $cm^{-1}$ wave numbers, and will mask electronic energy levels at certain magnetic fields and sample orientations. Cd-rich samples are thus not suitable for the present investigation.

The far-infrared absorption measurements were made using, first, a Fourier-transform Michelson interferometer and, second, the hydrogen-cyanide and deuterium-cyanide lasers. The interferometer was a Grubb Parsons Model with a germanium bolometer cooled to 1.3°K as a detector. The resolution in these broad-band studies was one or two wave numbers, and the signal-to-noise ratio in the interferogram using a 10-sec integration time was 25:1. A 1-mil beam divider was used to optimize spectral throughput in the 20–100 $cm^{-1}$ range, which experiments have shown to be the main region of interest.

The samples of ZnS:$Fe^{2+}$ were placed in a vertical light pipe between the interferometer and the detector and were immersed in liquid helium pumped to 1.3°K. The light pipe passed through the bore of a 15-T (150-kG) water-cooled Bitter solenoid magnet. The thickness of the 1-cm-diam cylindrical samples was

TABLE I. Impurity concentrations[a] in the single crystals of natural, cubic ZnS.

| | *SA*[b] | *U*[c] | *J*[d] |
|---|---|---|---|
| Fe | 40 | 45 | 350 |
| Cd | 15 | 80 | 45 |
| Cu | 2 | 0.6 | 1 |
| Oxygen | 100 | <50 | 70 |
| Others | <0.2 | <1 | <10 |

[a] The concentrations are given in units of $10^{18}$ atoms/$cm^3$. The Fe, Cd, Cu were measured with standard chemical techniques, the oxygen content was determined by neutron activation.
[b] *SA* (and *SB*) is from Picos de Europa, Santander, Spain (similar to sample *R*118 of Ref. 1).
[c] *U* is from Summit County, Colorado, U.S.A. (similar to sample *R*114 of Ref. 1).
[d] *J* is from Shiraita, Echigo, Japan (similar to sample *R*140 of Ref. 1).

adjusted to give about 50% absorption over the range 20–100 $cm^{-1}$, and was about 1 cm. The flat faces were polished to good optical finish with one face having a tilt to eliminate interference effects. Two samples were used with either a [001] or a [101] crystal axis parallel to the magnetic field. Optical-absorption curves were obtained for 0, 5.7, 10.1, and 13.9 T over the wave number range 10–100 $cm^{-1}$ for the [001] oriented sample, and for 0 and 10 T between 20–100 $cm^{-1}$ wave numbers for the [101] oriented sample. From these runs the optical-absorption coefficient $\alpha$ was computed using the expression

$$I=I_0(1-R)^2e^{-\alpha t}. \quad (1)$$

Here $I$ is the intensity of transmitted light, $I_0$ is the intensity of incident light, $R$ is the reflectivity of a single surface at normal incidence, and $t$ is the sample thickness. $R$ can be determined from the index of refraction or determined from our experiments in the low wave number region ($<25$ $cm^{-1}$) by assuming the absorption to be negligible outside the absorption peaks.

In addition to the above broad-band experiments a few measurements were made using 337 $\mu$m (29.67 $cm^{-1}$) and 194 $\mu$m (52.08 $cm^{-1}$) radiations from HCN and DCN lasers, respectively. The construction and operation of these lasers have been described elsewhere.[4,5] The samples were placed in a flow-through helium Dewar which could be cooled to about 5 or 6°K. The radiation was detected using Golay cells, and a 0–14-T magnet was used to obtain the resonance spectra.

## III. EXPERIMENTAL RESULTS

The optical-absorption coefficient $\alpha$ as a function of photon wave number $\bar{\nu}$ (measured in $cm^{-1}$) for the two different samples studied in magnetic fields is shown in Figs. 1 and 2. Figure 1 is for a [001] oriented sample (sample *SA*) and Fig. 2 is for a [101] oriented sample (sample *SB*). In both cases, the light was unpolarized and was propagating parallel to the magnetic field.

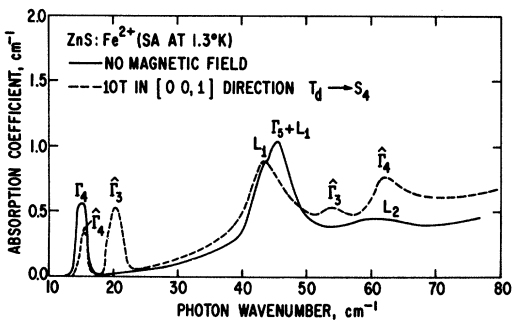


FIG. 1. Optical-absorption coefficient versus photon wave number for ZnS:$Fe^{2+}$ (*SA*) in 0 and 10 T magnetic induction at 1.3°K. The magnetic field is in the [001] direction and the light is unpolarized and propagating parallel to the magnetic field.

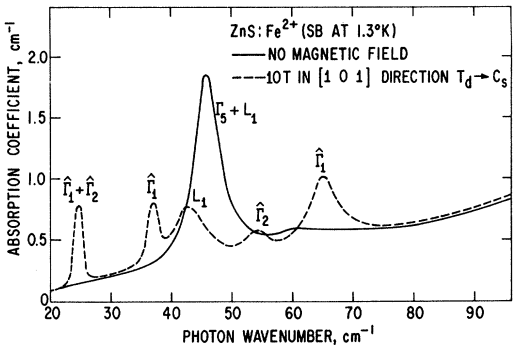


FIG. 2. Optical-absorption coefficient versus photon wave number for ZnS:$Fe^{2+}$ (*SB*) in 0 and 10 T magnetic induction at 1.3°K. The magnetic field is in the [101] direction and the light is unpolarized and propagating parallel to the magnetic field.

Since $\alpha$ is proportional to the $Fe^{2+}$ concentration, we notice that sample *SB* has a slightly higher $Fe^{2+}$ concentration than sample *SA*. Sample *SA* has been analyzed to contain $40\times10^{18}$ Fe and $15\times10^{18}$ Cd atoms/$cm^3$; see Table I. We assume that all of the Fe atoms enter the crystal substitutionally at Zn sites and are present as $Fe^{2+}$.

In the figures the electronic excitations are designated by $\Gamma$ or $\hat{\Gamma}$,[6] and local modes by $L$. $\Gamma_i$ (or $\hat{\Gamma}_i$) designates a transition from the ground state $\Gamma_1$ (or $\hat{\Gamma}_1$) to the state $\Gamma_i$ (or $\hat{\Gamma}_i$).

The origin of the local mode, $L_1$, at 43 $cm^{-1}$ wave number is uncertain, although it may be associated with oxygen or hydroxyl groups in the crystal; see Table I. It was not present in the synthetic ZnS studied by Kinch and DeWit; see Acknowledgments. The local mode $L_2$ at 63 $cm^{-1}$ wave number we believe is due to Cd. This mode is not as strong in the Spanish samples as in Cd-rich ($80\times10^{18}$ atoms/$cm^3$) samples from Colorado, U.S.A. (Fig. 3). This feature is also apparent in Figs. 1 and 2 of Ref. 1 and where $L_2$ was thought to be due to Fe. A comparison of the 63-$cm^{-1}$ band for samples *S* and *U*, see Fig. 3, and for sample *J*, see Fig. 2 of Ref. 1, shows that the absorption intensity of this band is roughly proportional to the Cd concentration given in Table I.

In Figs. 4 and 5 the results of the laser measurements are given. These results give additional information about the energy levels as well as some information about their magnetic-field dependence.

## IV. THEORY

### A. Crystal-Field Splittings

The purpose of this section is to derive the energy levels of $Fe^{2+}$ in a site of tetrahedral symmetry (point group $T_d$). The crystal field will split the lowest term, $^5D$, of the free $Fe^{2+}$ ion into an orbital doublet $^5E$ and an

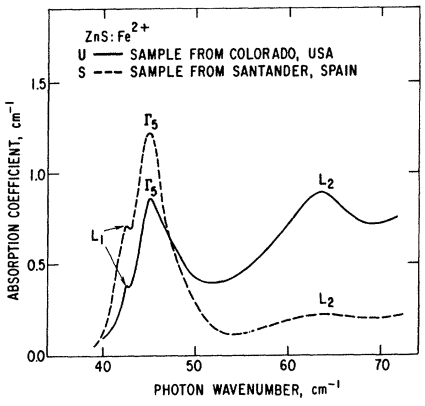


FIG. 3. Optical-absorption coefficient for natural ZnS at 4.2°K for samples $S$ and $U$ in zero magnetic field.

orbital triplet ${}^5T_2$. ${}^5E$ is the ground state and ${}^5T_2$ is higher in energy by the crystal-field splitting $\Delta(=10\,|\,Dq\,|)$.[2,7] To classify the wave functions according to their irreducible representations[6] we need only to consider their angular dependence. Using the Condon and Shortley[8] phase convention for the spherical harmonics $Y_L{}^M$ and with the [001] axis as the polar axis, see Fig. 14 of Ref. 2, we find[2,9]

$$E\begin{cases}|\,\theta\rangle = Y_2{}^0,\\ |\,\epsilon\rangle = (Y_2{}^2+Y_2{}^{-2})/\sqrt{2},\end{cases}$$

$$T_2\begin{cases}|\,\xi\rangle = i(Y_2{}^1+Y_2{}^{-1})/\sqrt{2},\\ |\,\eta\rangle = -(Y_2{}^1-Y_2{}^{-1})/\sqrt{2},\\ |\,\zeta\rangle = i(Y_2{}^2-Y_2{}^{-2})/\sqrt{2}.\end{cases} \tag{2}$$

The five spin functions $S_2{}^M$ $(M=0,\pm1,\pm2)$ may be classified in a similar way into $E$ or $\Gamma_3$ and $T_2$ or $\Gamma_5$ functions. The ten combined spin-orbit functions for the ${}^5E$ state, which we study in this investigation, form a basis for the following irreducible representations[2,10]:

$$E\times(E+T_2)=\Gamma_1+\Gamma_2+\Gamma_3+\Gamma_4+\Gamma_5. \tag{3}$$

The wave functions comprising these five different irreducible representations are obtained from the tables of coupling coefficients for the $T_d$ group given by Koster *et al.*[10] (Table II).

TABLE II. Explicit wave functions for the ten states comprising the five irreducible representations of the ${}^5E$ ground state of $Fe^{2+}$ in tetrahedral symmetry. (On the right-hand side of the above expressions the first label in each set denotes the orbital state, the second label denotes the spin state.)

| | |
|---|---|
| $\|\,\Gamma_1\rangle$ | $=(\,\|\,\theta\theta\rangle+\|\,\epsilon\epsilon\rangle)/\sqrt{2}$ |
| $\|\,\Gamma_2\rangle$ | $=(\,\|\,\theta\epsilon\rangle-\|\,\epsilon\theta\rangle)/\sqrt{2}$ |
| $\|\,\Gamma_3\theta\rangle$ | $=(-\|\,\theta\theta\rangle+\|\,\epsilon\epsilon\rangle)/\sqrt{2}$ |
| $\|\,\Gamma_3\epsilon\rangle$ | $=(\,\|\,\theta\epsilon\rangle+\|\,\epsilon\theta\rangle)/\sqrt{2}$ |
| $\|\,\Gamma_4X\rangle$ | $=(-\sqrt{3}\,\|\,\theta\xi\rangle-\|\,\epsilon\xi\rangle)/2$ |
| $\|\,\Gamma_4Y\rangle$ | $=(\sqrt{3}\,\|\,\theta\eta\rangle-\|\,\epsilon\eta\rangle)/2$ |
| $\|\,\Gamma_4Z\rangle$ | $=\|\,\epsilon\zeta\rangle$ |
| $\|\,\Gamma_5\xi\rangle$ | $=(\,\|\,\theta\xi\rangle-\sqrt{3}\,\|\,\epsilon\xi\rangle)/2$ |
| $\|\,\Gamma_5\eta\rangle$ | $=(\,\|\,\theta\eta\rangle+\sqrt{3}\,\|\,\epsilon\eta\rangle)/2$ |
| $\|\,\Gamma_5\zeta\rangle$ | $=-\|\,\theta\zeta\rangle$ |

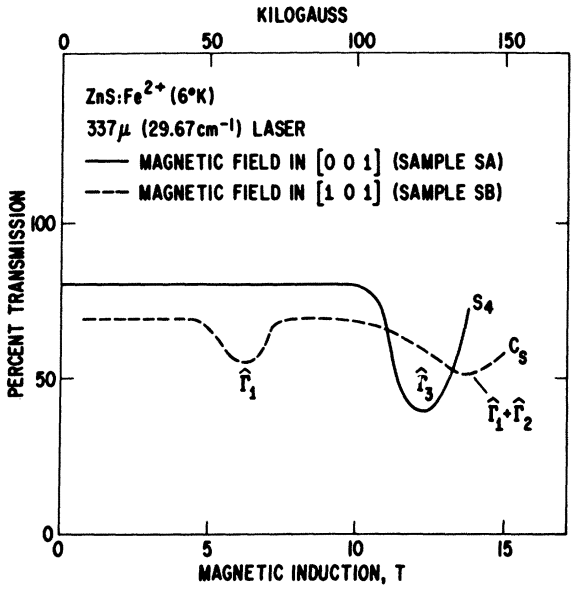


FIG. 4. Percent transmission for HCN laser through ZnS:$Fe^{2+}$ at 6°K for 1-cm-thick samples. The laser radiation is unpolarized and propagating parallel to the magnetic field.

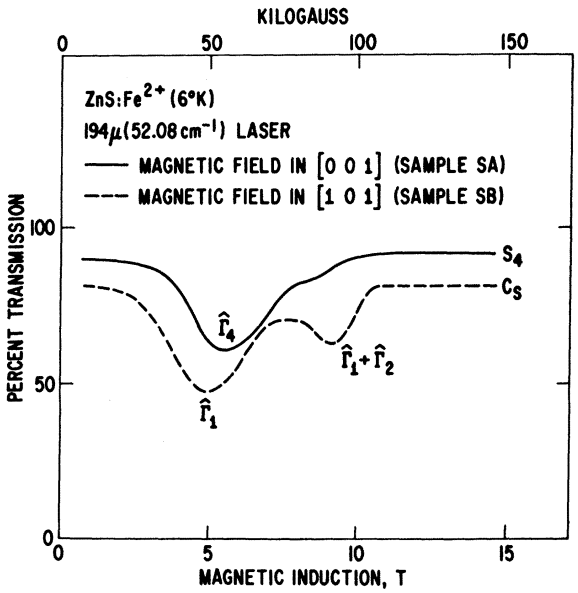


FIG. 5. Percent transmission for DCN laser through ZnS:$Fe^{2+}$ at 6°K for 1-cm-thick samples. The laser radiation is unpolarized and propagating parallel to the magnetic field.

Spin-orbit coupling does not split $^5E$ in first order but does so in second order mainly through coupling to the $^5T_2$ states. To the accuracy of second-order perturbation theory, this splitting is equivalent to that produced by the operator

$$\mathcal{H}_E=-\tfrac{1}{6}K\{[3S_z^2-S(S+1)]U_\theta+\sqrt{3}(S_x^2-S_y^2)U_\epsilon\} \quad (4)$$

acting within the $^5E$ wave functions. Here $\hbar\mathbf{S}$ is the spin operator with the components $S_x$, $S_y$, $S_z$ referred to the cubic axes. $U_\theta$ and $U_\epsilon$ are orbital operators[11] defined to have the following matrix representation within the orbital $^5E$ states $|\theta\rangle$ and $|\epsilon\rangle$:

$$U_\theta=\begin{pmatrix}-1 & 0\\ 0 & 1\end{pmatrix}, \qquad U_\epsilon=\begin{pmatrix}0 & 1\\ 1 & 0\end{pmatrix} \quad (5)$$

(i.e., $\langle\theta\,|\,U_\theta\,|\,\theta\rangle=-1$ etc.).

The coefficient $K$ in Eq. (4) has the value[3]

$$K=6[(\lambda^2/\Delta)-\rho]. \quad (6)$$

The first term in $K$ originates from the spin-orbit interaction ($=\lambda\mathbf{L}\cdot\mathbf{S}$) between $^5E$ and $^5T_2$. The second term is due to spin-spin interactions between the $^5E$ states and spin-orbit interaction with higher $LS$ terms of the $3d^6$ configuration.[12] The parameter $\rho$, introduced by Pryce,[13] has the value $+0.95$ cm$^{-1}$ for the free $Fe^{2+}$ ion.

The operator $\mathcal{H}_E$ will split the ten $^5E$ spin-orbit states into five uniformly spaced levels separated by the energy interval $K$. The singlet $\Gamma_1$ is the ground state. The next higher state is $\Gamma_4$, a triplet; and then follows $\Gamma_3$, a doublet; $\Gamma_5$, a triplet; and $\Gamma_2$, a singlet; as shown in Figs. 6–8 at zero magnetic induction.

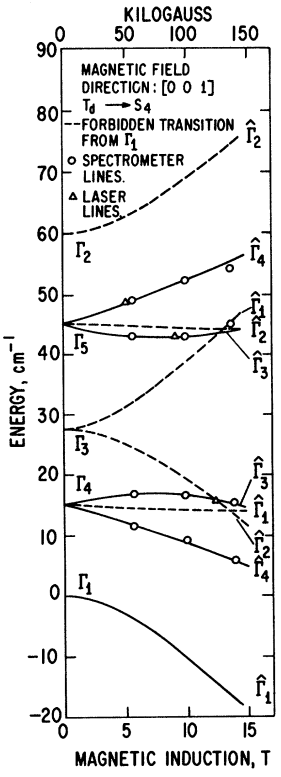


FIG. 6. Energy levels of ZnS:Fe$^{2+}$ versus magnetic induction in [001] direction. The symmetry is lowered by the magnetic field from $T_d$ to $S_4$ and the $i$th irreducible representation of $S_4$ is designated by $\hat{\Gamma}_i$. The lines represent theoretical values, the circles experimental points obtained from spectrometer runs and the triangles points obtained from laser experiments. Transitions from the ground state to the dashed states are symmetry forbidden.

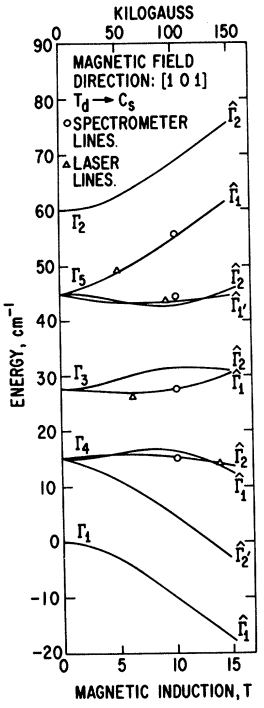


FIG. 7. Energy levels of ZnS:Fe$^{2+}$ versus magnetic induction in [101] direction. The symmetry is lowered by the magnetic field from $T_d$ to $C_s$ and the $i$th irreducible representation of $C_s$ is designated by $\hat{\Gamma}_i$. The lines represent theoretical values, the circles represent experimental points obtained from spectrometer runs, and the triangles represent points obtained from laser experiments.

### B. Zeeman Interaction

In a magnetic field the Hamiltonian will also include the term

$$\mathcal{H}_z=\mu_B\mathbf{B}\cdot(\mathbf{L}+2\mathbf{S}). \quad (7)$$

$\mu_B$ is the Bohr magneton and $\mathbf{B}$ the magnetic induction. However, the magnetization ($=\mathbf{M}$) of ZnS is very small compared to the magnetizing fields ($\mathbf{H}$) produced by the laboratory magnets, and we can therefore set

$$\mathbf{B}=\mu_0\mathbf{H}, \quad (8)$$

where $\mu_0$ is the permeability of free space.

Since the orbital angular momentum operator $\mathbf{L}$ has only zero matrix elements within the $^5E$ states, we have for the Zeeman interaction simply $\mathcal{H}_z=\mu_B\mathbf{B}\cdot 2\mathbf{S}$ when we neglect spin-orbit coupling with the $^5T_2$ states.

If, however, this coupling is taken into account, the Zeeman interaction will take the form[11]

$$\mathcal{H}_z=\tfrac{1}{2}\mu_B[2g_1(\mathbf{S}\cdot\mathbf{B})+g_2\{[3S_zB_z-(\mathbf{S}\cdot\mathbf{B})]U_\theta +\sqrt{3}[S_xB_x-S_yB_y]U_\epsilon\}]. \quad (9)$$

To second order in perturbation theory, the spin-orbit coupling between $^5E$ and $^5T_2$ will give

$$g_1=2-(4\lambda/\Delta), \qquad g_2=-(4\lambda/\Delta). \quad (10)$$

TABLE III. The matrix representation of $\mathcal{H}_z$ using the ten functions of Table II as a basis.

$$A_j=-i(g_1+g_2)\beta B_j/\sqrt{2}, \quad D_j=-i(g_1-g_2)\beta B_j/\sqrt{2}, \quad C_j=-i\sqrt{3}g_1\beta B_j/2,$$
$$E_j=-i(g_1+2g_2)\beta B_j/2, \quad F_j=-i(g_1-2g_2)\beta B_j/2,$$

$j=x$, $y$, or $z$ and $B_j$ is the component of the magnetic induction along the $j$ axis. In the calculations for Figs. 6–11 we have used Eq. (10) with $\lambda=-73$ cm$^{-1}$, $\Delta=3400$ cm$^{-1}$ to give $\lambda/\Delta=-0.0214$.

| $\vert\Gamma_1\rangle$ | $\vert\Gamma_4X\rangle$ | $\vert\Gamma_4Y\rangle$ | $\vert\Gamma_4Z\rangle$ | $\vert\Gamma_3\theta\rangle$ | $\vert\Gamma_3\epsilon\rangle$ | $\vert\Gamma_5\xi\rangle$ | $\vert\Gamma_5\eta\rangle$ | $\vert\Gamma_5\zeta\rangle$ | $\vert\Gamma_2\rangle$ |
|---|---|---|---|---|---|---|---|---|---|
| 0 | $2A_x$ | $2A_y$ | $2A_z$ | 0 | 0 | 0 | 0 | 0 | 0 |
| | 0 | $F_z$ | $-F_y$ | $A_x$ | $-\sqrt{3}A_x$ | 0 | $C_z$ | $C_y$ | 0 |
| | | 0 | $F_x$ | $A_y$ | $+\sqrt{3}A_y$ | $C_z$ | 0 | $C_x$ | 0 |
| | | | 0 | $-2A_z$ | 0 | $C_y$ | $C_x$ | 0 | 0 |
| | | | | 0 | 0 | $+\sqrt{3}D_x$ | $-\sqrt{3}D_y$ | 0 | 0 |
| | | | | | 0 | $D_x$ | $D_y$ | $-2D_z$ | 0 |
| | Complex conjugate | | | | | 0 | $E_z$ | $-E_y$ | $2D_x$ |
| | | | | | | | 0 | $E_x$ | $2D_y$ |
| | | | | | | | | 0 | $2D_z$ |
| | | | | | | | | | 0 |

The matrix representations of $\mathcal{H}_z$ within the ten $^5E$ states are given in Table III for an arbitrary direction of the vector **B**.

### C. Oscillator Strength

The oscillator strength $f(A, B)$ for the transition $A\rightarrow B$ generally consists of two parts:

$$f(A, B)=f_e(A, B)+f_m(A, B). \quad (11)$$

The first term, $f_e(A, B)$, arises from electric dipole transitions and the second term, $f_m(A, B)$, arises from magnetic dipole transitions. It is convenient to express these oscillator strengths as

$$f_e(A, B)=C_e p_e(A, B),$$
$$f_m(A, B)=C_m p_m(A, B). \quad (12)$$

$C_e$ and $C_m$ are constants characteristic for the system studied and $p_e$ and $p_m$ are relative oscillator-strength parameters. These parameters as well as a detailed treatment of transitions probabilities are given elsewhere[1] for the case of zero magnetic field. In that case Eq. (12) only contained one of the two terms $f_e(A, B)$ or $f_m(A, B)$.

In the presence of a magnetic field the remaining degeneracies of the five $^5E$ levels are lifted and considerable mixing of the zero-field wave functions occurs. The ground state ($=\psi_0$) will for an arbitrary magnetic-field direction be some linear combination of the ten $^5E$ wave functions $\phi_1, \phi_2, \ldots, \phi_{10}$. Thus

$$\psi_0=\sum_{i=1}^{10} c_i\phi_i, \quad (13)$$

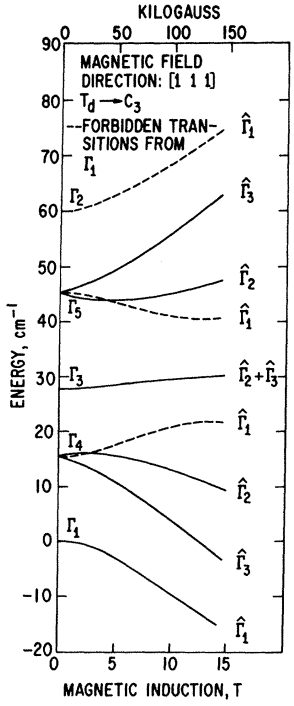


FIG. 8. Energy levels of ZnS:$Fe^{2+}$ versus magnetic induction in [111] direction. The symmetry is lowered by the magnetic field from $T_d$ to $C_3$ and the $i$th irreducible representation of $C_3$ is designated by $\hat{\Gamma}_i$. The lines represent theoretical values. No experiments were made for this orientation.

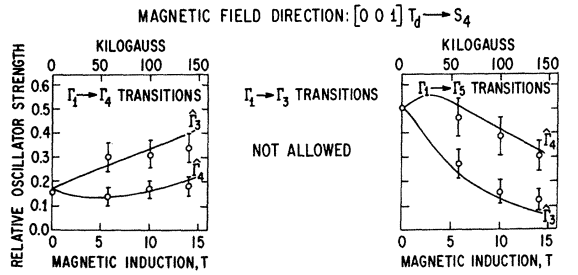


FIG. 9. Relative oscillator strengths $f_r$, for optical transitions versus magnetic field in [001] direction. The light is unpolarized and propagating parallel to the magnetic field. The lines represent theoretical values; the circles with error bars represent the experimental points.

where $c_i$ is, in general, complex, and

$$\sum_{i=1}^{10} c_i^* c_i = 1. \quad (14)$$

In a similar fashion the excited states $\psi_e$ are expressed as linear combinations of the $\phi_i$. To determine $p_e$ and $p_m$ in Eq. (12), we need to evaluate matrix elements of the form

$$\langle \psi_e \mid \mathcal{O} \mid \psi_0 \rangle = \sum_{j,i} c_j^* c_i \langle \phi_j \mid \mathcal{O} \mid \phi_i \rangle, \quad (15)$$

where $\mathcal{O}$ is the operator causing the optical transition.

## V. INTERPRETATION AND DISCUSSION OF EXPERIMENTAL AND THEORETICAL RESULTS

### A. Zero Magnetic Field

An investigation of the far-infrared optical absorption of ZnS:Fe$^{2+}$ in zero magnetic field has been made earlier by Slack, Roberts, and Ham.[1] Our experimental results are essentially in agreement with these authors although we have modified their interpretations.

At liquid-helium temperatures, almost all the Fe$^{2+}$ ions are in the ground-state singlet $\Gamma_1$. In zero magnetic field there are only two allowed transitions from this state,[1] a magnetic dipole transition to the $\Gamma_4$ triplet and an electric dipole transition to the $\Gamma_5$ triplet (Figs. 9–11 for $\mathbf{B}=0$). From our measurements (Fig. 1 and Fig. 2 for $\mathbf{B}=0$) we obtain $\Gamma_4$ to be $15.0\pm0.1$ cm$^{-1}$ above the ground state with a half-width of 2 cm$^{-1}$. The absorption band at 45 cm$^{-1}$ wave number is found to consist of both a local mode $L_1$ and the $\Gamma_1 \rightarrow \Gamma_5$ transition. $\Gamma_5$ is $45.0\pm0.2$ cm$^{-1}$ above the ground state with a half-width of 4.5 cm$^{-1}$. These results give an experimental value for the coefficient $K$ in Eq. (4) of $K=15.0\pm0.1$ cm$^{-1}$. The integral $\int \alpha(\bar{\nu}) d\bar{\nu}$ for $L_1$ at 43 cm$^{-1}$ is 2.4 cm$^{-2}$ for sample $SA$ and 1.4 cm$^{-2}$ for sample $U$, and we find that $L_1$ is associated with some impurity in the crystal other than Fe. It may be associated with oxygen or hydroxyl groups in the crystal; see Table I. We have also established that the absorption at 63 cm$^{-1}$ wave number is a local mode $L_2$. The intensity of $L_2$ is proportional to the Cd concentration, and we therefore assign this absorption to a local mode of Cd (Fig. 3).

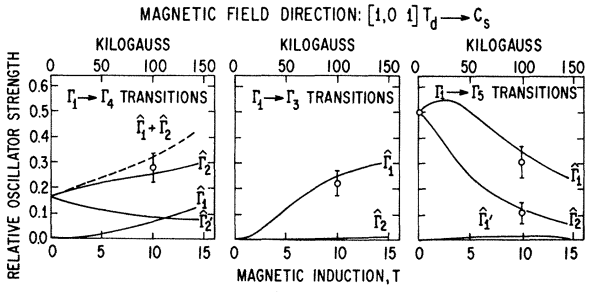


FIG. 10. Relative oscillator strengths $f_r$, for optical transitions versus magnetic field in [101] direction. The light is unpolarized and propagating parallel to the magnetic field. The lines represent theoretical values, the circles with error bars the experimental points.

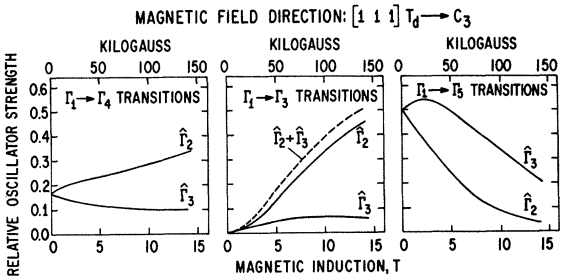


FIG. 11. Relative oscillator strengths $f_r$, for optical transitions versus magnetic field in [111] direction. The light is unpolarized and propagating parallel to the magnetic field. The lines represent theoretical values. No experiments were made for this orientation.

Realizing that part of the 45 cm$^{-1}$ wave number band of Ref. 1 is due to a local mode, we have reevaluated the electric dipole strength parameter $C_e$. We obtain for our Spanish samples ($SA$ and $SB$) $C_e=1.3\times10^{-9}$ as compared to the value $C_e=3.1\times10^{-9}$ given earlier.[1] This agrees favorably with sample $U$, for which the local mode absorption $L_1$ is quite small, and with sample $J$ (see Table IV).

A theoretical estimate of $C_e$ can be made based on the total oscillator strength of the $^5E \rightarrow {}^5T_2$ absorption band in the near infrared and the spin-orbit admixture of the $^5T_2$ wave functions to the $^5E$ states.[1] If we assume that the splitting of the orbital $^5E$ states is entirely due to spin-orbit coupling with the $^5T_2$ states [$\rho=0$ in Eq. (6)] we get $C_e=5.5\times10^{-9}$. (This is obtained with $\lambda=-92$ cm$^{-1}$, $\Delta=3400$ cm$^{-1}$, and $\rho=0$. These values give $K=15.0$ cm$^{-1}$, which is equal to the experimentally determined value of $K$.) If, however, part of the splitting is due to an effective spin-spin interaction, $\rho\neq0$, we obtain a theoretical value of $C_e=3.7\times10^{-9}$. (This is obtained with $\lambda=-73$ cm$^{-1}$, $\Delta=3400$ cm$^{-1}$, and $\rho=+0.95$ cm$^{-1}$. These values also give $K=15.0$ cm$^{-1}$.) The theoretical value of $C_e$ would be still further reduced in the presence of a dynamic Jahn-Teller effect.[3] In that case a pure electronic transition will be shared between different vibronic states. We have made an estimate of this reduction by assuming that the coupling coefficient for Fe$^{2+}$ to the lattice is the same in ZnS as in CdTe.[3] The reduction in oscillator strength is found to be 20% for the electric dipole transition ($\Gamma_1 \rightarrow \Gamma_5$) and 30% for the magnetic dipole transition ($\Gamma_1 \rightarrow \Gamma_5$). These results are given in Table IV. We observe that the agreement between predicted and observed oscillator strengths is good for the magnetic dipole transition while the agreement for the electric dipole transition is not completely satisfactory.

### B. Magnetic Field in [001] Direction

With a magnetic field in the [001] direction, the symmetry of Fe$^{2+}$ is lowered from $T_d$ to $S_4$.[10] The point

TABLE IV. Experimental and theoretical values for the electric and magnetic dipole oscillator strength parameters $C_e$ and $C_m$ for optical transitions within ${}^5E$.

| | $10^9 C_e$ | $10^9 C_m$ |
|---|---|---|
| Sample $S$[a] | 1.3 | 1.1 |
| Sample $J$[a] | 1.2 | 1.0 |
| Sample $U$[a] | 1.2 | 1.1 |
| Theory 1[b] | 5.5 | 1.7 |
| Theory 2[c] | 3.7 | 1.7 |
| Theory 3[d] | 3.0 | 1.2 |

[a] See Table I.
[b] No spin-spin coupling, no Jahn-Teller coupling.
[c] Spin-spin coupling, no Jahn-Teller coupling.
[d] Spin-spin coupling and Jahn-Teller coupling.

group $S_4$ contains only one-dimensional representations, and therefore all remaining zero-field degeneracies are lifted. We have calculated the eigenenergies by diagonalizing the matrix in Table III. In Fig. 6 we have plotted the calculated energies, assuming $K=15.0$ cm$^{-1}$, and have also given the experimental points. With the unpolarized light propagating parallel to the magnetic field, the electric and magnetic dipole operators will have components only in the $xy$ plane and transitions from the $\Gamma_1$ ground state will only be allowed to $\hat{\Gamma}_3$ and $\hat{\Gamma}_4$ states. Thus the upper $\hat{\Gamma}_1$, $\hat{\Gamma}_2$ levels are shown as dashed lines in Fig. 6.

In calculating the oscillator strengths for the different allowed transitions, we have set $C_e=C_m$ because experimentally $C_e \approx C_m$ (Table IV). We also define a relative oscillator strength $f_r$ for the $A \rightarrow B$ transition by

$$f_r(A, B)=f(A, B)/f(\Gamma_1, \Gamma_5), \qquad (16)$$

where $f(\Gamma_1, \Gamma_5)$ is the oscillator strength of the $\Gamma_1 \rightarrow \Gamma_5$ transition in zero magnetic field. The relative oscillator strength for the magnetic-dipole transition $\Gamma_1 \rightarrow \Gamma_4$ will then be $f_r(\Gamma_1, \Gamma_4)=\frac{1}{3}$ in zero magnetic field (see Fig. 3 of Ref. 1).

Calculations of oscillator strengths have been made for unpolarized light. We have obtained our results by adding the results from two perpendicular, linearly polarized beams. The corresponding operators and their transformation properties are given in Table V. Results from these calculations together with experimental points are given in Fig. 9. The experimental points are obtained from measuring $\int \alpha(\bar{\nu}) d\bar{\nu}$. The error bars in Fig. 9 indicate the experimental uncertainty in this integration.

### C. Magnetic Field in [101] Direction

With a magnetic field in the [101] direction the symmetry of the $Fe^{2+}$ ion is changed from $T_d$ to $C_s$. All zero-field degeneracies are lifted, and transitions from the $\hat{\Gamma}_1$ ground state to all excited states will be symmetry allowed.

The energies were obtained by diagonalizing the matrix of Table III with $B_x=B_z=|\mathbf{B}|/\sqrt{2}$ and $B_y=0$. To calculate relative oscillator strengths we used the operators of Table V. The calculated energies and oscillator strengths together with experimental data points are given in Figs. 7 and 10.

The $\Gamma_1 \rightarrow \Gamma_3$ transition is forbidden for $\mathbf{B}=0$. For $\mathbf{B}$ in the [101] direction it is allowed for $|\mathbf{B}|>0$, thus we can find the energy of the middle or $\Gamma_3$ level. In the center panel of Fig. 10 we show the $f_r$ for the two transitions from $\Gamma_1$ to $\Gamma_3$. The $f_r$ ($\hat{\Gamma}_1$, $\hat{\Gamma}_1$) here is appreciable, and we see both the laser and spectrometer lines. However, in $C_s$ symmetry the $f_r$ ($\hat{\Gamma}_1$, $\hat{\Gamma}_2$) is very small and only reaches the value of 0.01 at 15 T. Therefore this transition is too weak to be observed in our experiments. To be able to fit the experimental data we have to assume the $\Gamma_3$ state to be $27.5 \pm 0.5$ cm$^{-1}$ wave number above the ground state in zero magnetic field; the others are at $K$, $3K$, and $4K$ ($K=15.0$ cm$^{-1}$). A uniform spacing $K$ of the energy levels would predict $\Gamma_3$ to be 30 cm$^{-1}$ above the ground state. A nonuniform splitting of the energy levels in zero magnetic field as found in our experiment could be obtained by including higher-order terms in perturbation theory.[2] It could also be obtained by the introduction of a dynamic Jahn-Teller coupling.[3] We do not believe that the departure

TABLE V. Transformation properties of electric and magnetic dipole operators used in calculating relative oscillator strengths.

| Magnetic field and light direction | Polarization[a] | Operators[b] Electric dipole | Magnetic dipole |
|---|---|---|---|
| [001] | 1 | $R_\xi$ | $S_y$ |
| | 2 | $R_\eta$ | $S_x$ |
| [101] | 1 | $R_\eta$ | $(S_x-S_z)/\sqrt{2}$ |
| | 2 | $(R_\xi-R_\zeta)/\sqrt{2}$ | $S_y$ |
| [111] | 1 | $(R_\eta-R_\xi)/\sqrt{2}$ | $(2S_x-S_y-S_z)/6^{1/2}$ |
| | 2 | $(2R_\xi-R_\eta-R_\zeta)/6^{1/2}$ | $(S_y-S_z)/\sqrt{2}$ |

[a] 1 and 2 are the two perpendicular linearly polarized light beams.
[b] $(R_\xi, R_\eta, R_\zeta)$ are the $x$, $y$, and $z$ components of the electric dipole operator $R$, and $(S_x, S_y, S_z)$ are components of the magnetic dipole operator.

from uniform splitting in zero magnetic field is significant enough to call for further detailed studies.

The $\Gamma_1 \rightarrow \Gamma_2$ transition is forbidden for $\mathbf{B}=0$ and for $|\mathbf{B}|>0$ when $\mathbf{B}$ is in the [001] direction and in the [111] direction. For $\mathbf{B}$ in the [101] direction it is allowed for $|B|>0$; see the highest level in Fig. 7. Our calculation of the $f_r$ $(\hat{\Gamma}_1, \hat{\Gamma}_2)$ of this highest transition in $C_s$ symmetry shows that $f_r$ $(\hat{\Gamma}_1, \Gamma_2)$ is very small and only reaches the value of 0.002 at 15 T. This transition is therefore too weak to be observed in our experiments, so we have no experimental datum for the position of the $\Gamma_2$ level in zero field.

### D. Magnetic Field in [111] Direction

No experiments were made with the magnetic field in the [111] direction. For the sake of completeness we have given the calculated energy levels and relative oscillator strengths in Figs. 8 and 11.

### E. Laser Results

The half-width for the laser lines, $\Delta B_L$, is related to the half-width of the absorption lines, $\Delta\bar{\nu}$, though the relation

$$\Delta\bar{\nu} \cong (\partial\bar{\nu}/\partial B)\Delta B_L. \qquad (17)$$

The quantities $\Delta\bar{\nu}$ and $\Delta B_L$ are obtained in our experiments, and we get an experimental value of $\partial\bar{\nu}/\partial B$ which can be compared with our theoretical calculations. The magnetic linewidth $\Delta B_L$ is 1.5 T for the 29.67 $cm^{-1}$ resonances and 2.5 T for the 52.08 $cm^{-1}$ resonances (Figs. 4 and 5). The experimental values obtained for $\partial\bar{\nu}/\partial B$ agree well with theoretical values calculated from the slopes of the $\bar{\nu}$-versus-$B$ curves in Figs. 6–8.

### ACKNOWLEDGMENTS

We are grateful to Professor B. Lax and J. Button for the use of the far-infrared spectroscopy and magnetic field facilities of the Francis Bitter National Magnet Laboratory, MIT. We are also indebted to Dr. L. Neuringer of the National Magnet Laboratory, who encouraged us to do these experiments, to T. Bernstein for making some of the spectrometer runs, to Dr. S. Roberts for making available far-infrared optical-absorption data on Cd-rich ZnS samples, to Dr. M. Kinch and Dr. M. deWit for communicating to us the results of some of their magneto-optical studies on synthetic ZnS:$Fe^{2+}$ (made by Dr. J. Schneider) in the [111] direction prior to publication, and to Dr. F. S. Ham for valuable discussions and for comments on the manuscript.

* Permanent address: National Physical Laboratory, Teddington, Middlesex, England.

[1] G. A. Slack, S. Roberts, and F. S. Ham, Phys. Rev. **155,** 170 (1967).

[2] G. A. Slack, S. Roberts, and J. T. Vallin, Phys. Rev. **187,** 511 (1969).

[3] J. T. Vallin, Phys. Rev. B **2,** 2390 (1970).

[4] C. C. Bradley, K. J. Button, B. Lax, and L. Rubin, I.E.E.E. J. Quantum Electron. **4,** 733 (1968).

[5] C. C. Bradley and K. J. Button, in Air Force Report No. AMICOM DAAH03-69-C-0436, 1969 (unpublished).

[6] We use interchangeably the notation ($A_1$, $A_2$, $E$, $T_1$, $T_2$) of Mulliken [R. S. Mulliken, Phys. Rev. **43,** 279 (1933)] and the notation ($\Gamma_1$, $\Gamma_2$, $\Gamma_3$, $\Gamma_4$, $\Gamma_5$) of Bethe [H. A. Bethe, Ann. Physik **3,** 133 (1929); see also Ref. 10, pp. 88–101] to denote the irreducible representations of $T_d$. We use Mulliken's notation in particular for orbital electronic states and Bethe's notation for spin-orbit states. $\hat{\Gamma}$ denotes an irreducible representation of a subgroup of $T_d$ corresponding to the reduction in symmetry obtained in the presence of a magnetic field.

[7] W. Low and M. Weger, Phys. Rev. **118,** 1119 (1960).

[8] E. U. Condon and G. H. Shortley, *The Theory of Atomic Spectra* (Cambridge U. P., London, 1935), p. 193.

[9] Throughout the paper the notation $\theta$, $\epsilon$ is used to designate partner functions (or operators) belonging to $\Gamma_3$ and transforming, respectively, as $[2z^2-(x^2+y^2)]$ and $\sqrt{3}[x^2-y^2]$, while $\xi$, $\eta$, $\zeta$ designate those belonging to $\Gamma_5$ or $T_2$ and transforming as $yz$, $xz$, $xy$ [or equivalently under $T_d$ as $x$, $y$, $z$], and $X$, $Y$, $Z$ designate partners belonging to $\Gamma_4$ or $T_1$ and transforming like the angular momentum components $L_X$, $L_Y$, $L_Z$.

[10] G. F. Koster, J. O. Dimmock, R. G. Wheeler, and H. Statz, *Properties of the Thirty-two Point Groups* (MIT Press, Cambridge, Mass., 1963).

[11] F. S. Ham, Phys. Rev. **166,** 307 (1968).

[12] R. E. Trees, Phys. Rev. **82,** 683 (1951).

[13] M. H. L. Pryce, Phys. Rev. **80,** 1107 (1950).